Supplementary Materials for

Wavefront-Selective Fano Resonant Metasurfaces

Adam Overvig[1] and Andrea Alù[1,2*]

[1]Photonics Initiative, Advanced Science Research Center at the Graduate Center of the City University of New York

[2]Physics Program, Graduate Center, City University of New York

1. Meta-unit design

The focus of the main text is to explore the novel physics enabled by aperiodic perturbations applied to otherwise high-symmetry photonic crystal slabs (in particular, the consequent wavefront-selectivity). To demonstrate these phenomena and concepts, we employ the meta-unit geometries originally proposed in Ref. [26] of the main text, and validate the concepts using full-wave simulations (finite difference time domain, by Lumerical Solutions). Here, we briefly review the properties of the specific unit cell designs, but note that since the origin of these phenomena are in symmetries, this is just one example system and other unit cell designs may also be employed.

Figures S1(a,b) depict the basic geometry of a unit cell of the proposed device, consisting of two layers of elliptical inclusions. Sitting on a substrate with $n_1 = 1.45$, the metasurface is composed of two tightly stacked thin films with $n_2 = 3.45$, each etched with elliptical holes with dimensions $80 \times 340 nm$, spaced with pitch $a = 400 nm$. In each layer, the two ellipses have a fixed relative orientation of $90°$ relative to each other, and an angle α relative to the lattice coordinates. The top layer is a similar pair of ellipses oriented at $90°$ relative to each other, with an orientation

relative to the first layer of $\Delta\alpha$. But for the $90°$ relative orientation of adjacent ellipses, the unit cell fit within a square lattice. The dimerization in the x direction makes the unit cell rectangular by doubling the period in the x direction but not the y direction. In reciprocal space, this implies Brillouin zone folding, halving the first Brillouin zone in the k_x direction [Fig. S1(c)]. Figures S1(d,e) show the reflectance due to RCP incident light for plane waves with varying k_y ($k_x = 0$) and varying k_x ($k_y = 0$), respectively. The Fano resonance follows the band structure of the q-BIC, thereby demonstrating selectivity in the momentum-frequency domain. The band-edge mode is circled in white, and the magnetic field profile of this mode is shown in Figs. S1(f-h).
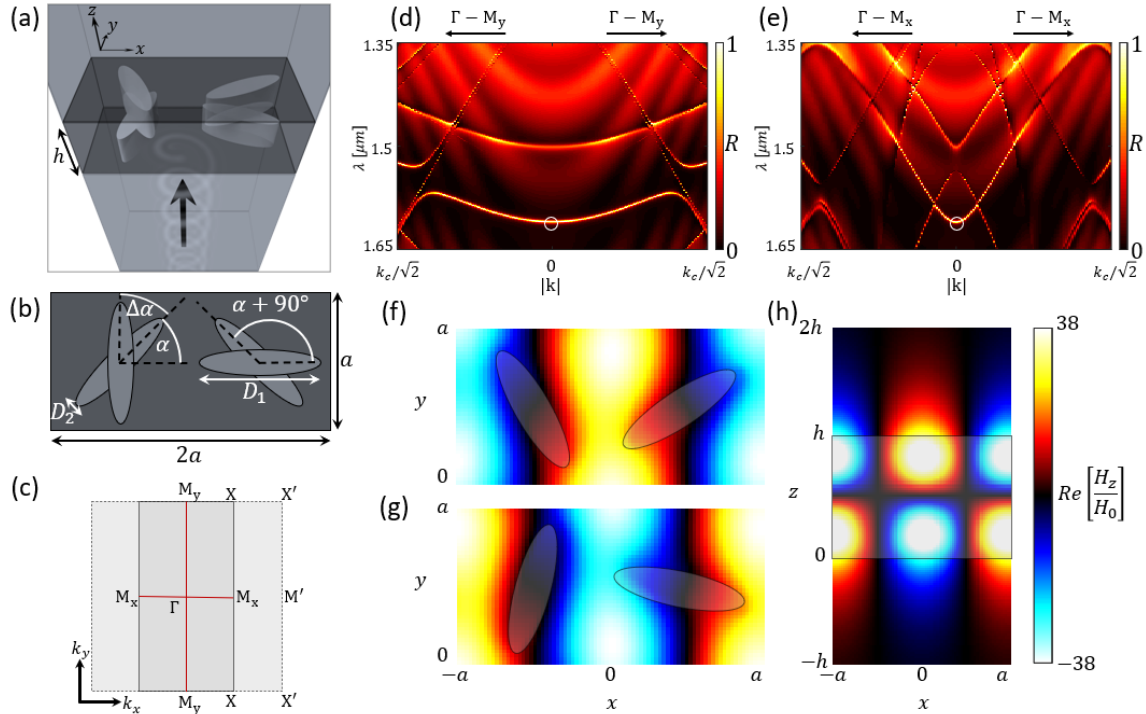
Fig. S1. (a) Schematic of the chiral metasurface unit cell. (b) Top-view, defining the orientation angles of the two layers. (c) First Brillouin Zone of the unperturbed (light gray, primed labels) and perturbed (gray, unprimed labels) unit cell. (d,e) Reflectance when RCP light is incident, showing the angular response in the y-direction and x-direction. $k_c = 2\pi/1.485\,\mu m$, meaning the largest incident k-vectors correspond to light incident at 45 degrees for $\lambda = 1.485\,\mu m$. The band-edge mode is circle in white. Magnetic field profiles (xy cuts) of the band-edge mode are shown at (f) the top interface at $z = h$, (g) the bottom interface at $z = 0$. (h) The magnetic field profile (xz cut) at $y = 0$.

Last, we note that the values of α and $\Delta\alpha$ alter the Q-factor and resonant frequency of the q-BIC slightly. This may be corrected for by adjusting $D_{avg} = (D_1 + D_2)/2$ to correct the resonant frequency while adjusting $\delta = D_1 - D_2$ to correct for the Q-factor. In practice, we find that such adjustments are not necessary to demonstrate the wavefront-selectivity concept in the main text. However, such optimization could further improve our results, and may be necessary in other similar systems (especially with higher Q-factor).

2. Potential fabrication process

While the main result of the main text is to conceptually extend the optical Fano resonance from the momentum-frequency domain to the space-frequency domain, we also numerically explored concrete systems to enable these phenomena, composed of two planarized layers. While separate from the theoretical results of the work, here we discuss a potential fabrication method capable of realizing these devices for operation in the near-infrared. We also note that operation in the microwave spectrum would greatly increase ease of fabrication for proof-of-concept devices, since the feature sizes need not be microscopic (and, for instance, 3D printing may be employed).

Figure S2 presents a flow-chart of a potential fabrication process, using standard micro-fabrication techniques and materials. The device is composed of two planar layers, which may be fabricated successively. The patterning method may be a standard electron-beam lithography approach wherein a resist is exposed, chemically developed, and used as an etching mask for the underlying silicon layer. After the first layer is patterned, the remaining resist must be removed and the filler material (SiO_2) deposited (for instance, by chemical vapor deposition, physical vapor deposition, or a spin-on-glass). This layer is then planarized (sometimes automatically achieved by spin-on-glasses, otherwise achievable by a variety of means such as chemical-mechanical

polishing or repeated deposition and etching). Then, the second layer of a-Si is deposited (such as by chemical vapor deposition) and an identical electron-beam lithography process is carried out for the second layer. Alignment marks made in the first lithography enable the accurate alignment of the underlying layer's pattern and the second patterning step, with routine alignment accuracies achievable within $40nm$. Finally, the device is finished by depositing a thick layer of SiO_2 as the superstrate.
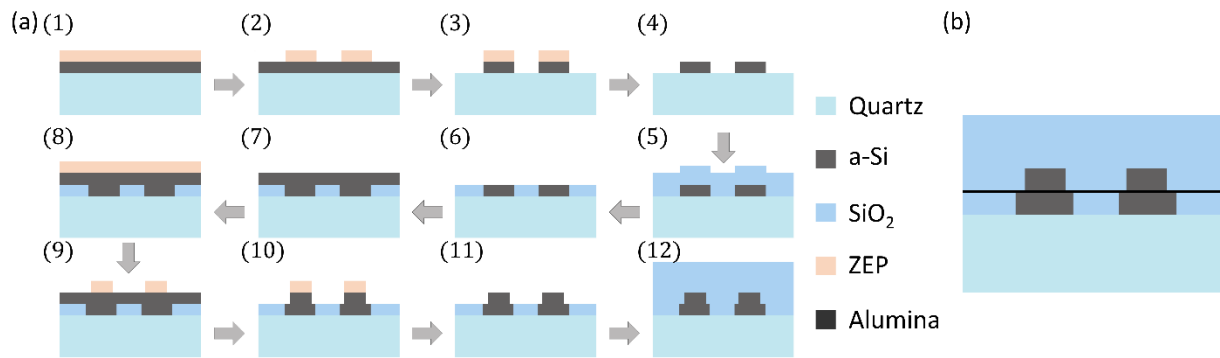
Fig. S2. (a) Proposed fabrication flow using multi-step lithography and planarization. (1) A thin layer of resist (ZEP) is spun on a thin film of a-Si sitting on a quartz substrate. (2) Electron-beam lithography and development patterns the resist, which is then (3) transferred to the a-Si layer by reactive ion etching. (4) The remaining resist is removed by chemical means and SiO_2 is deposited and (6) planarized. (7) Another a-Si layer and (8) resist layer are added and (9) exposed. (10) The pattern is transferred to the second layer and (11) the remaining resist is chemically removed. (12) Finally, glass is deposited, overfilling the device. (b) Example final result altering the process in (a) to include the deposition of an etch-stop layer of Alumina between steps (6) and (7).

We note that this process flow is just one example. Alternatives (such as lift-off of an etching mask) may be explored as well to improve the reliability. For instance, the height of the filler material need not be zero as drawn in step (6) of Fig. 2 and assumed in the devices in the main text. So long as the two layers are closely spaced compared to the wavelength, the phenomena we explore here will be observable. This freedom also allows for a deposition of an etch-stop layer (a standard choice being alumina) between steps (6) and (7), removing the need for precise timing in

the etching step (10). Shown in Fig. S2(b), this thin dielectric material does not alter the physics of interest, here, and the impact on the optical response (resonant frequency, Q-factor, etc.) may easily be accounted for in full-wave simulations.
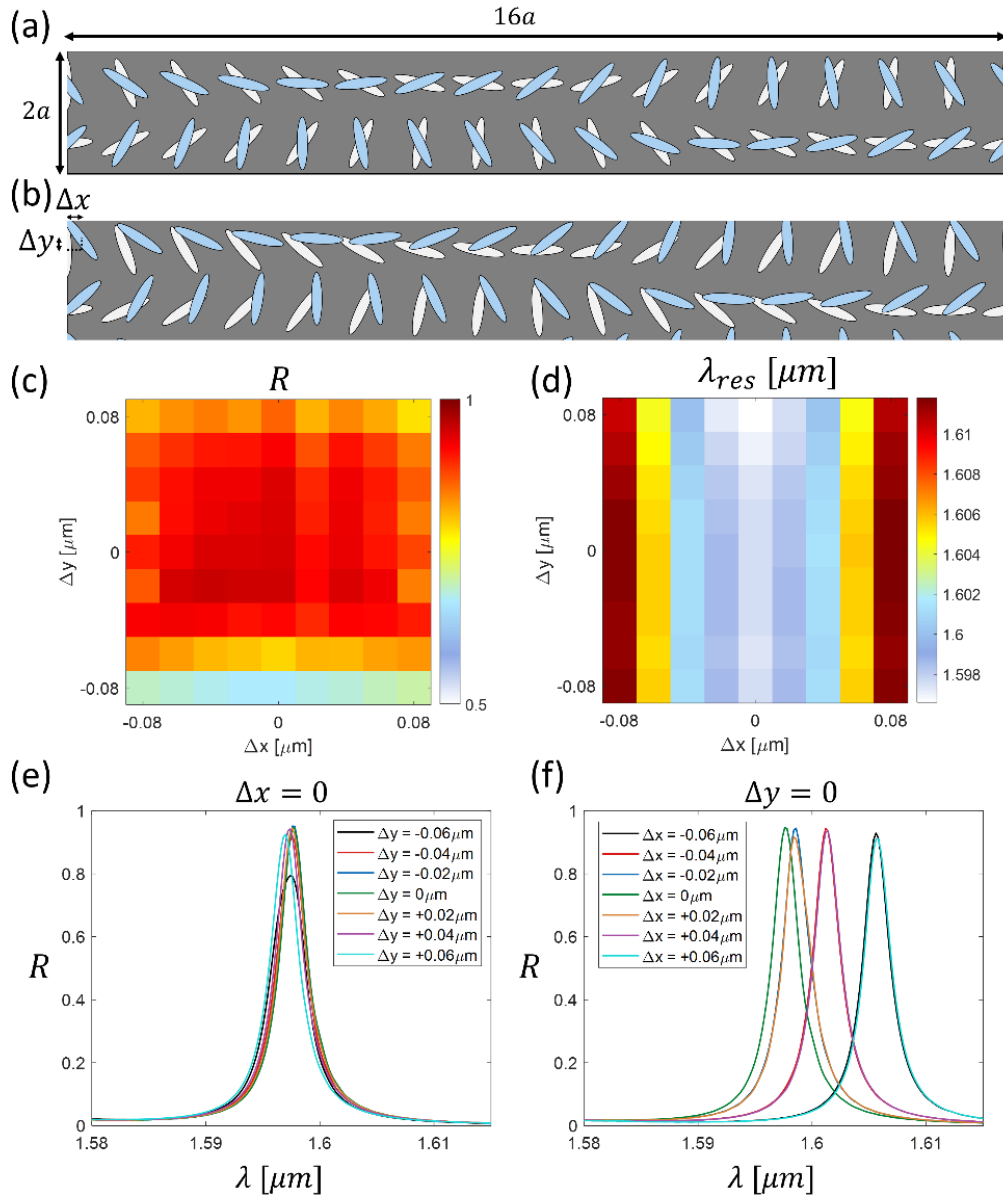
Fig. S3. Study on reflectance and resonant wavelength as a function of misalignment of top and bottom layers. (a) Ideal geometry of the phase gradient device, with the top layer of elliptical holes highlighted blue. (b) Device geometry with the top layer misaligned in the x and y directions, with magnitudes Δx and Δy, respectively. (c,d) Peak reflectance and resonant wavelength as a function of the misalignment. (e,f) Example spectra showing the impact of shifts in the x and y directions.

3. Study on alignment

In Fig. S3, we briefly study the most significant obstacle of the fabrication flow presented above: alignment of the two layers. As an example, we perform full-wave simulations of the phase-gradient metasurface device in Fig. 2 of the main text, but with the top layer displaced from the bottom layer. Alignment is routinely achievable within 40nm, but to better explore the robustness, we study shifts in both the x and y directions ranging from -80nm to +80nm.